PNAS INAUGURAL ARTICLE | APPLIED PHYSICAL SCIENCES

Plausible photomolecular effect leading to water evaporation exceeding the thermal limit

Yaodong Tu[a,b], Jiawei Zhou[a], Shaoting Lin[a], Mohammed Alshrah[a], Xuanhe Zhao[a], and Gang Chen[a,1]

This contribution is part of the special series of Inaugural Articles by members of the National Academy of Sciences elected in 2023.
Contributed by Gang Chen; received July 26, 2023; accepted September 25, 2023; reviewed by Xiulin Ruan and Shannon K. Yee

We report in this work several unexpected experimental observations on evaporation from hydrogels under visible light illumination. 1) Partially wetted hydrogels become absorbing in the visible spectral range, where the absorption by both the water and the hydrogel materials is negligible. 2) Illumination of hydrogel under solar or visible-spectrum light-emitting diode leads to evaporation rates exceeding the thermal evaporation limit, even in hydrogels without additional absorbers. 3) The evaporation rates are wavelength dependent, peaking at 520 nm. 4) Temperature of the vapor phase becomes cooler under light illumination and shows a flat region due to breaking-up of the clusters that saturates air. And 5) vapor phase transmission spectra under light show new features and peak shifts. We interpret these observations by introducing the hypothesis that photons in the visible spectrum can cleave water clusters off surfaces due to large electrical field gradients and quadrupole force on molecular clusters. We call the light-induced evaporation process the photomolecular effect. The photomolecular evaporation might be happening widely in nature, potentially impacting climate and plants' growth, and can be exploited for clean water and energy technologies.

evaporation | hydrogel | photomolecular | photothermal | solar

Evaporation of water by sunlight is one of the most pervasive phenomena in nature and daily life, having both fundamental and practical importance in science and technology (1–5). Because water absorbs little sunlight in the visible spectrum (6, 7), absorbing materials such as carbon black are used to absorb sunlight and heat water for thermal evaporation (8, 9). Solar evaporation rates using porous absorbers have been observed to exceed the theoretical thermal evaporation limit (5, 10–21), but the mechanism of this phenomenon remains unclear. Here, we report surprising experimental observations leading us to hypothesize direct light-induced evaporation in which a photon cleaves off water clusters from water–vapor interfaces without going through a normal thermal evaporation process, which we call the photomolecular effect. Our key observations are as follows. First, we find that partially wetted hydrogels absorb visible spectrum light despite their constituent materials being nonabsorbing in the same wavelength range. Second, we demonstrate that water evaporation rates from hydrogels without additional absorption materials under visible light illumination such as light-emitting diode (LED) exceed the thermal limit. Third, the highest evaporation rate happens with green LED, when water is least absorbing, while the measured absorptance does not show much wavelength dependence in the visible spectrum. Fourth, the vapor above the hydrogel is cooler under light compared to without light, and the temperature distribution shows the saturation region. Fifth, the transmission spectra of the vapor phase above the evaporating surface under LED radiation show new features and peak shift compared with no LED illumination. The photomolecular effect bears similarities to the photoelectric effect (22, 23), but with two significant differences: i) It happens in the spectrum where bulk water does not absorb and ii) one photon can cleave off a cluster of water molecules, which can lead to evaporation rate exceeding the thermal limit. Such a photomolecular evaporation process could be happening widely in nature. It may significantly impact the earth's water cycle, climate change, and has potential clean water and energy technology applications.

The theoretical limit for thermal evaporation, using solar or light-emitting diodes energy or electrical sources, can be calculated from $J_{t,\max} = q/[L + c_p(T_s - T_w)]$, where q is the solar flux or other forms of input power per unit surface area, L the latent heat, c_p the constant-pressure specific heat, and T_s and T_w are the evaporating surface temperature and bulk water temperatures, respectively. The denominator is the amount of heat needed to change one kilogram of water from the liquid to the vapor state. Taking $T_s = 40\ ^\circ\mathrm{C}$ and $T_w = 20\ ^\circ\mathrm{C}$, and standard solar flux at one sun $q = 1\ \mathrm{kW/m^2}$, the

Significance

Water evaporation under sunlight is a pervasive phenomenon, having both fundamental and practical importance in science and technology. Solar-driven evaporation rates using porous absorbers have been reported to exceed the theoretical thermal evaporation limit, but the mechanism of this phenomenon remains unclear. Here, we hypothesize that a photon can cleave off water clusters from water–vapor interfaces and call this process the photomolecular effect, in analogy to the well-known photoelectric effect. We provide experimental evidence and explain the physical driving force supporting this hypothesis. Such photomolecular evaporation process could be happening widely in nature. It may significantly impact the earth's water cycle, climate change, and has potential clean water and energy technology applications.

Reviewers: X.R., Purdue University; and S.K.Y., Georgia Tech.

The authors declare no competing interest.

Copyright © 2023 the Author(s). Published by PNAS. This article is distributed under Creative Commons Attribution-NonCommercial-NoDerivatives License 4.0 (CC BY-NC-ND).

[1]To whom correspondence may be addressed. Email: gchen2@mit.edu.

This article contains supporting information online at https://www.pnas.org/lookup/suppl/doi:10.1073/pnas.2312751120/-/DCSupplemental.

Published October 30, 2023.

Downloaded from https://www.pnas.org by CAS DALIAN INSTITUTE CHEMICAL PHYSICS on July 29, 2025 from IP address 119.78.131.176.

thermal evaporation limit is $J_{t,\max} = 1.45\ \mathrm{kg/(m^2h)}$, assuming all solar energy is converted into heat and used for water evaporation. Experimentally, $J_{\max}$ as high as $4-5\ \mathrm{kg/(m^2h)}$ (15, 18) and over $7\ \mathrm{kg/(m^2h)}$ (16, 20) in two- and three-dimensional structures had been reported, respectively. Different materials, from polyvinyl alcohol (PVA) to other polymers (14, 16, 18) and even inorganic porous absorbers (13, 17, 20, 21), have shown this effect. These works either impregnate absorbers such as conducting polymers or light-absorbing nanoparticles into porous structures or directly use porous absorbers such as via carbonizing plants. The most-cited mechanism for the higher evaporation rate than the theoretical thermal limit is reduced latent heat of the water in these materials (5, 10, 12), based on a theoretical picture of different water states inside hydrogel: bound water, intermediate water, and free water (24, 25). Experimental evidence for this mechanism includes 1) reduced latent heat of evaporation measured by differential scanning calorimetry (DSC) and 2) higher evaporation rate of hydrogel samples in dark compared to pure water surface. However, DSC measured latent heat reduction is less than 30% which can be explained by the pressure increase inside hydrogel (26), and the higher dark evaporation rate can be explained by the increased surface area. The original publication mentioned the possibility of water evaporating as clusters (5), but there was no mechanism to support such a possibility. We show below experimental evidence that supports our photomolecular effect hypothesis: that photons can cleave off water clusters directly from water–vapor interfaces without going through thermal processes, which leads to water evaporation rate under solar and narrow spectrum LED radiation exceeding the theoretical thermal evaporation limits.

Results

Details of the synthesis and experimental procedures are provided in *Materials and Methods* and *SI Appendix*. We synthesized three types of porous PVA hydrogel samples: 1) pure PVA samples that do not include any additional absorbers, which are denoted as pure-PVA, 2) PVA samples integrated with polypyrrole (ppy) denoted as PVA-ppy, and 3) pure PVA coated on porous carbon paper, denoted as PVA-carbon. The synthesis involves freeze–thawing or freeze–drying to form proper porous structures (Fig. 1 *A* and *B*, *Preparation of Freeze-thawed and Freeze-dried Pure-PVA Samples*, *Preparation of Freeze-dried PVA Samples with PPy Absorber*, *Preparation of PVA-Carbon Sample*, and *Sample Characterization*, and *SI Appendix*, Figs. S1 and S2 and Notes S1–S3). We used DSC and thermal gravimetric analysis (TGA) to characterize their thermal properties (*SI Appendix*, Fig. S3 and Notes S4 and S5).

High Absorptance from Nonabsorbing Materials. We extract absorptance of different samples from measured reflectance and transmittance using an integrating sphere (Fig. 1*C*, *UV-VIS-NIR Absorptance Measurement*, and *SI Appendix*, Figs. S4–S7). Fig. 1*D* shows that the absorptances of pure water, dry PVA powder, the solution before forming the gel, and the as-gelated samples are close to zero, consistent with expectation. Surprisingly, although the freeze-thawed samples (Fig. 1*D* and *SI Appendix*, Fig. S6) still have about the same amount of water as the as-gelated sample, their absorptance increased significantly. Similarly, freeze-dried pure-PVA samples with different amounts of water become absorbing, although dry pure-PVA is not absorbing (Fig. 1 *E* and *F* and *SI Appendix*, Fig. S7). Considering that the multiple scattering effects can increase absorption pathlength by a maximum of $4n^2$,

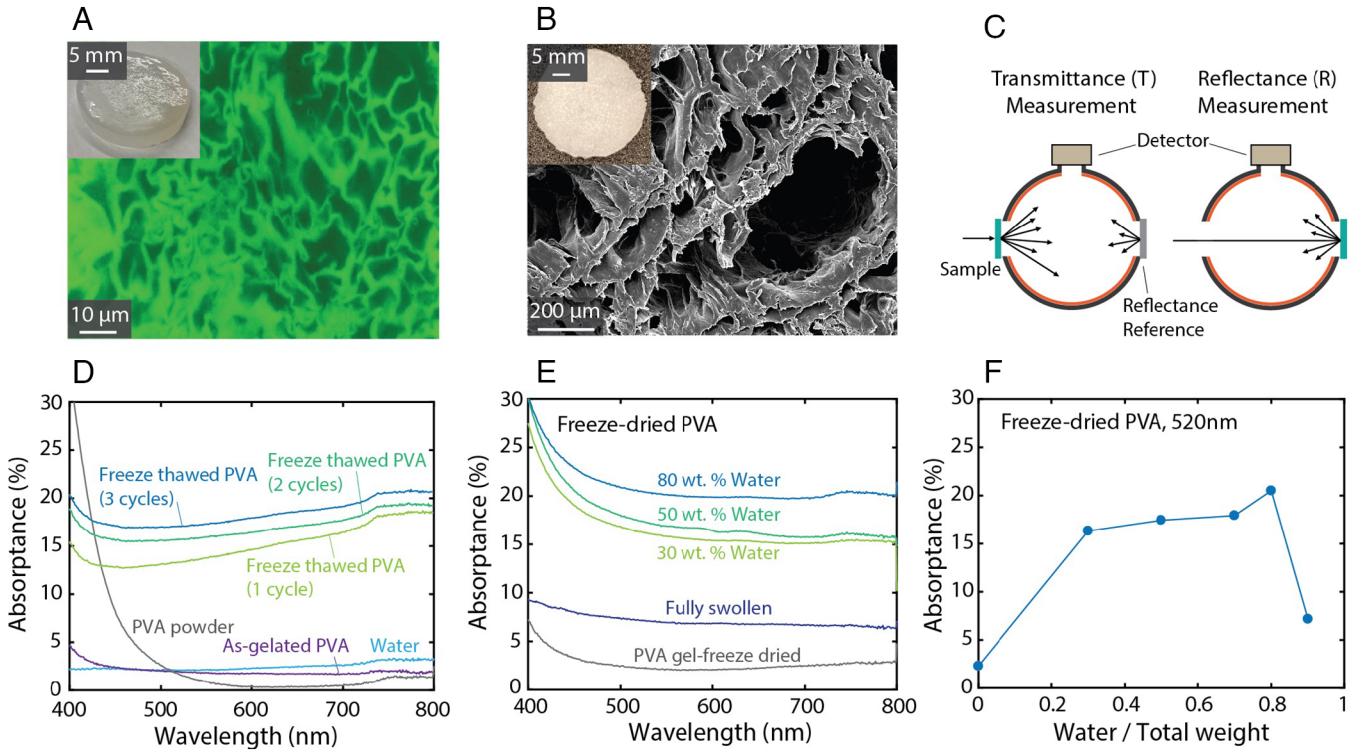

Fig. 1. Visible light absorption of hydrogels with different water contents. (*A*) Photo and confocal microscope image of a wet pure-PVA sample. (*B*) Photo and SEM image of a freeze-dried pure-ppy sample. (*C*) Illustration of integrating sphere measurements of absorptance by measuring reflectance and transmittance. (*D* and *E*) Measured absorptance of different samples. Although pure water, pure PVA solution and as-gelated pure-PVA samples do not absorb in the visible range, the freeze-thawed and freeze-dried pure-PVA samples have significant absorptance due to the photomolecular effect. (*F*) Absorptance of freeze-dried pure-PVA samples as a function of the water content at 520 nm, showing that absorptance depends on water contents.

Downloaded from https://www.pnas.org by CAS DALIAN INSTITUTE CHEMICAL PHYSICS on July 29, 2025 from IP address 119.78.131.176.

where n is the refractive index (27) (~1.33 for both water and polymers), the significant absorption cannot be explained by the light trapping effect.

The Hypothesis of the Photomolecular Effect. The surprising absorption in the freeze-thawed and freeze-dried pure-PVA samples containing some water can be explained by invoking a photomolecular effect which we will describe here and support with more experiments and theoretical arguments later. Inside bulk water, minimal absorption exists in the visible spectrum (6, 7), with a 40-m penetration depth at 500 nm. The photon energies are too high for the intramolecular vibrational modes and too low for electron transition. In water, hydrogen bond dominates, with typical bonding energy of 0.22 – 0.26 eV (28). It is well known that water molecules form a fluctuating hydrogen bond network, i.e., clusters, although the exact pictures, such as the clusters' size, shape, and lifetime, are still under debate (28–34). Theoretically, a photon can cleave off several water molecules together as a cluster by breaking bonds between the cluster and the rest of the water. For example, a photon at 500 nm with an energy of 2.48 eV can cleave off ~10 or even more intermolecular water bonds, depending on whether these are hydrogen bonds or even weaker van der Waals bonds. However, in bulk water, there is no space for the cluster to escape, i.e., the final states are occupied, so the process is forbidden.

On the other hand, this process can happen at the surface or in internal voids in the liquids. In freeze-dried pure-PVA samples with controlled water contents, there are high water–vapor interface areas for photons to directly cleave off water clusters, which enter the air, leading to measurable absorption (Fig. 1*F* and *SI Appendix*, Fig. S7). In freeze-thawed samples, internal voids allow the water clusters to be cleaved off and recondense (Fig. 1*E* and *SI Appendix*, Fig. S6). Next, we will show more experimental evidence supporting the photomolecular mechanism, followed by further discussion of the physical picture.

Evidence from Evaporation Rate. Fig. 2*A* shows the evaporation measurement setup (*Evaporation Rate Measurement* and *SI Appendix*, Fig. S8 and Note S7). Fig. 2 *B* and *C* illustrate the typical evaporation histories of hydrogel samples under solar radiation. The evaporation has two stages. The evaporation rate is below the thermal limit in the initial stage because the sample's surface under testing is still flooded with water (*SI Appendix*, Fig. S8*C*). It is the normal thermal evaporation stage, and the evaporation rate never exceeds the thermal limit. The second evaporation stage commences when the water surface recesses below the sample top surface (*SI Appendix*, Fig. S8*D*). In this stage, the measured evaporation rates of both PVA-ppy and PVA-carbon samples exceed the thermal evaporation limit (Fig. 2*D*). The evaporation rate of the pure-PVA sample is below the limit due to low absorptance (Fig. 1 *E* and *F*). Noted that we do not know the exact absorptance because we cannot measure the real water content of the top surface of the pure-PVA hydrogel evaporator in operation. However, after normalizing to its maximum absorptance of 20% as shown in Fig. 1*F*, it is even higher than that of the PVA-ppy and PVA-carbon samples. In Fig. 2*C*, we also show that evaporation from PVA-carbon samples never exceeds the thermal limit when the solar radiation is illuminated on the backside of the sample because absorption in the carbon substrate leads to thermal evaporation (*SI Appendix*, Fig. S10). We used LED lamps of different wavelengths to carry out evaporation tests and found that the evaporation rates in stage 2 depend on wavelengths (Fig. 2 *E* and *F*), with a peak rate at 520 nm. The sample's absorptance does not have peaks in the visible spectrum (Fig. 1*D* and *SI Appendix*, Fig. S9 *A* and *B*), while its surface temperature monotonically increases with wavelengths.

We interpret the peak evaporation rate at 520-nm wavelength to be due to the match of the photon energy with the bonding energy of the water clusters with surrounding molecules. The lower evaporation rate under shorter wavelength lights could be the competition between the photomolecular and photothermal effects. Light with a short wavelength has fewer photons under the same energy flux, and the excess photon energy will convert into clusters' kinetic energy. At longer wavelengths, the lower evaporation rates could be due to smaller clusters that can be excited by one photon. Further increase in wavelength leads to photothermal heating due to bulk water absorption.

We also tested the evaporation rate under different solar intensities. Interestingly, at lower light intensity, the evaporation rate normalized to the light intensity is higher than that at a higher one (Fig. 2 *G* and *H*), consistent with the picture that photomolecular and photothermal processes contribute to the evaporation. Evaporation from the pure-PVA sample under 0.1 sun green LED leads to a surface temperature of 21.5 °C, lower than the ambient temperature of 22.4 °C.

We also tested purely thermal evaporation by embedded electrical heaters inside the sample (*Electrical Heating* and *SI Appendix*, Fig. S10). The evaporation rate never exceeds the thermal limit. Fig. 2*I* compares the weight loss of the same sample under solar radiation and Joule heating with the same surface temperatures. It shows that solar heating reaches the steady state much faster than Joule heating and has a higher evaporation rate, demonstrating the difference between photomolecular and thermal evaporation.

Evidence from Vapor Phase Temperature Distribution. We further measured vapor layer temperature distributions and transmittance spectra to corroborate the cluster mechanism (*Temperature Measurements* and *SI Appendix*, Figs. S11 and S12 and Note S8). Fig. 3*A* shows the temperature distribution in the vapor phase when the light is on and immediately after the light is turned off for a PVA-ppy sample (*SI Appendix*, Fig. S11). The vapor temperature is actually lower when the light is on than when the light is off. Furthermore, when the light is on, the vapor temperature drop within the first 2 mm above the sample surface (Region I) is much faster than immediately after the light is off with an identical sample surface temperature (~35.4 °C). The temperature distributions above the surface between solar heating and Joule heating show similar contrasting behavior (Fig. 3*B*, *Temperature Measurements*, and *SI Appendix*, Fig. S12): sharp drop under solar irradiation near the surface while much slower change when light is off. Interestingly, the temperature distribution between 6 and 13 mm above the samples (Region II) is almost constant under solar irradiation in PVA-ppy and pure-PVA samples before it starts to drop again (Region III). In contrast, thermal evaporation from the pure water surface at a similar evaporation surface temperature (~35.8 °C) does not exhibit this flat region, as expected for normal thermal evaporation (Fig. 3*C*).

We interpret the sharp temperature drop in Region I to be due to the dissociation of water clusters when they collide with air molecules and absorb heat. This dissociation also leads to lower vapor phase temperature than when light is off. The flat temperature region (Region II) exists after air becomes saturated such that clusters break and renucleate (Fig. 3*D*). We can see condensation on a glass slide under green light (1 sun) over a PVA-ppy sample (Movie S1), even though the surface temperature is only ~42 °C. In Region III, air becomes unsaturated due to supply of fresh air from ambient.

Evidence from Vapor Phase Absorption Spectra. Fig. 3*E* shows transmission spectra of light in the vapor phase measured with the beam at different heights above the evaporating surface from

Downloaded from https://www.pnas.org by CAS DALIAN INSTITUTE CHEMICAL PHYSICS on July 29, 2025 from IP address 119.78.131.176.

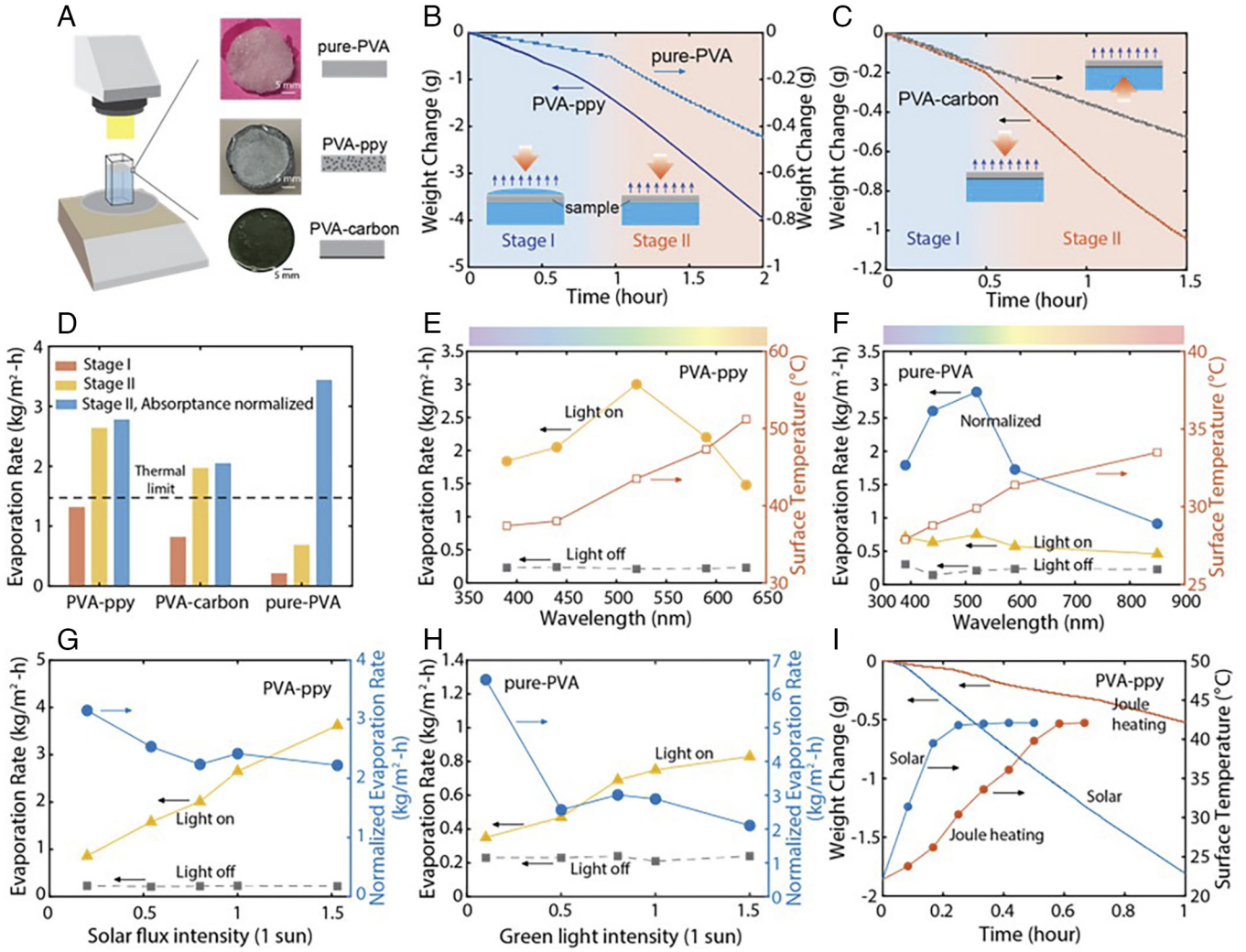

Fig. 2. Peculiarities of light-driven hydrogel evaporation. (*A*) Evaporation rate measurement platform and sample photos. (*B*) Weight change as a function time for a pure-PVA and a PVA-ppy sample under one sun, showing two stages. In stage I, water floods sample surface and the evaporation rate is lower than the thermal limit. This is the thermal evaporation stage. In stage II, water recesses into pores and evaporation rate increases significantly, exceeding the thermal limit. This stage has both photomolecular and thermal evaporation. (*C*) Weight change as a function of time for PVA-carbon under one sun irradiation from front and from back. Front illumination shows similar two stages as in *B*, while back illumination only shows thermal evaporation. (*D*) Comparison of evaporation rates under one sun in stage I and stage II among different samples, clearly showing stage II evaporation rates exceed the thermal limit. (*E* and *F*) Evaporation rate variation with wavelengths using LED radiation under one-sun equivalent intensity for PVA-ppy (*E*) and pure-PVA samples (*F*), both showing a peak rate at 520 nm (color bar indicates actual color at the corresponding wavelength). Surface temperatures are also shown. (*G*) Measured evaporation rates of a PVA-ppy sample under solar irradiation with different solar intensities, showing higher normalized rates at lower intensity. (*H*) Measured evaporation rate of a pure-PVA sample under green (520 nm) LED illumination, again showing higher rates at lower intensities. (*I*) Weight change and surface temperature as a function of time for a PVA-ppy sample under solar irradiation and electrical heating with the same evaporation temperatures. It takes much longer to reach steady surface temperature with Joule heating. Here, the normalized evaporation rates are obtained with the measured evaporation rates divided by the input energy which are calculated by the incident light intensity and the samples' absorptance (~93% for PVA-ppy, ~96% for PVA coated carbon paper as shown in *SI Appendix*, Fig. S9. And the absorptance under different wavelengths for pure-PVA is obtained from Fig. 1*E* by assuming the water content of the top surface of the evaporator in operation is 80%).

different samples (*Direct Transmission Spectrum of Vapor Phase* and *SI Appendix*, Fig. S13 and Note S9) and Fig. 3*F* compares the spectra of different samples at the same height, focusing on a narrow spectrum region near the fundamental OH vibrational band (more data are provided in *SI Appendix*, Fig. S14 and Datasets S1–S4). Water clusters are challenging to create, to measure, and to interpret (35–38). However, we do notice some features suggesting clusters' existence. First, we notice that the prominent peaks do not change with heights for pure water. Second, we notice that a new absorption feature appears at 3,612 cm^{-1}, and the peak locations shifts ~ 2 cm^{-1}. Third, the peak between 3,620 and 3,630 cm^{-1} also shifts for vapor above hydrogels, compared to that above pure water. Although we cannot say more about size clusters and the measurement is complicated by the experiment done in open air, we interpret these as signs of clusters' existence and their dissociation in the vapor phase. The fact that we can directly observe the vapor spectra change above evaporating sample surfaces indicates the abundance of the clusters.

Discussion

Driving Force for the Photomolecular Effect. While a photon cleaving off a molecular cluster can meet the energy conservation requirement, a key question is what is the driving force for the photomolecular effect? According to the Maxwell equations (39), the perpendicular component of the displacement field should be continuous, i.e., $\varepsilon_1 E_{1\perp} = \varepsilon_2 E_{2\perp}$, where the dielectric constant $\varepsilon_1 = 1$ and $\varepsilon_2 = 1.8$ for air and water, respectively. This boundary condition implies a discontinuity of the electric field, which is, of course, a mathematical simplification. In reality, the field changes

Downloaded from https://www.pnas.org by CAS DALIAN INSTITUTE CHEMICAL PHYSICS on July 29, 2025 from IP address 119.78.131.176.

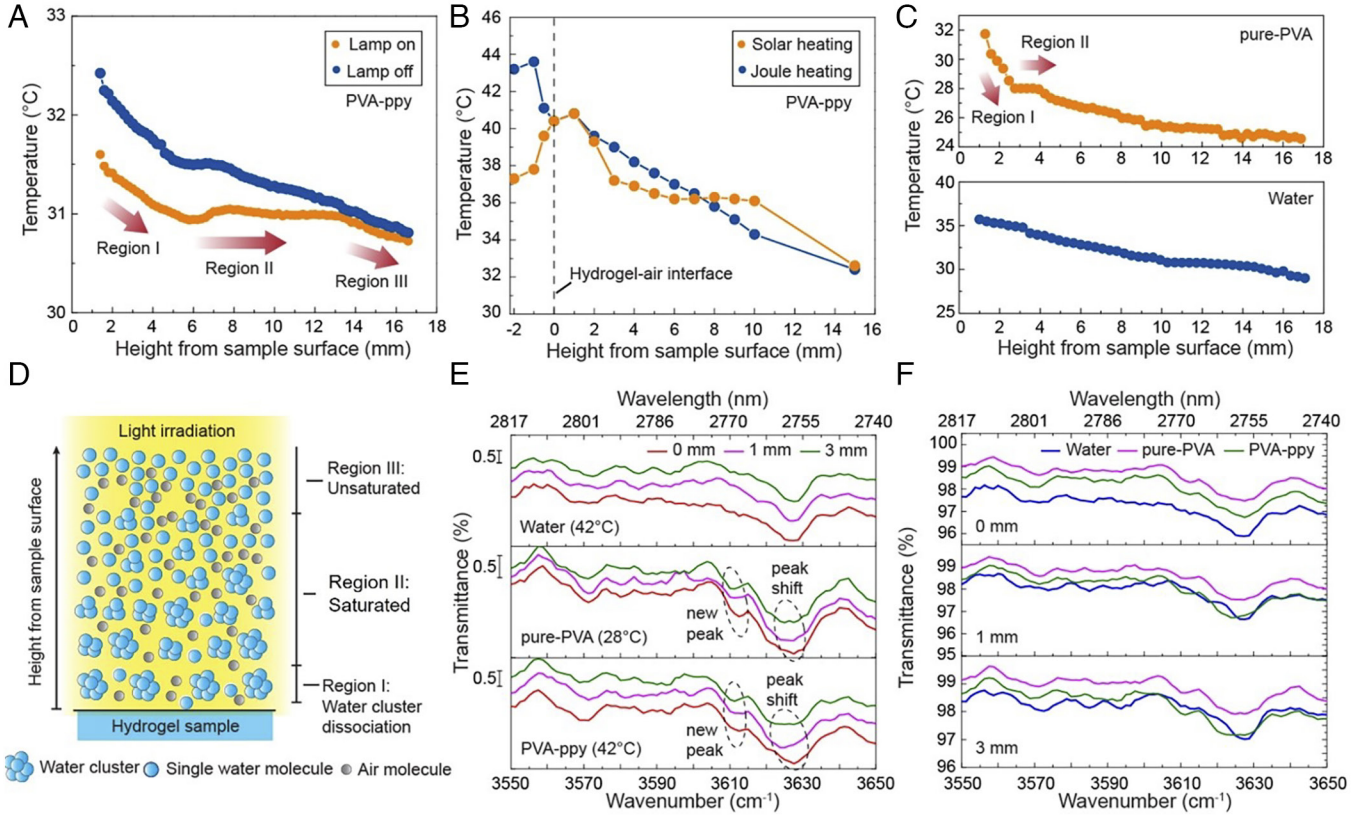

Fig. 3. Dissociation of water clusters in vapor phase. (*A*) Vapor phase temperature distributions above the PVA-ppy sample measured with the IR camera when the lamp is on, which shows a sharp temperature drop region (Region I) and a flat temperature region (Region II), and immediately after the lamp is turned off, for which temperature variation is nearly linear. (*B*) Vapor phase temperature distributions of a PVA-ppy sample measured using a thermocouple under solar heating, which is similar to that in *A* with temperature peaks near surface region, and electrical heating, which shows temperature peaks inside and vapor phase temperature distribution similar to lamp off in *A*. (*C*) Comparison of vapor-phase temperature for pure-PVA sample and pure water under green LED, showing similar behavior as (*A*) for the PVA-ppy sample under light. The pure water sample has an absorber attached to bottom and sample surface was controlled to be at the same temperature as pure-PVA sample by adjusting the solar intensity. The vapor phase temperature distribution is like lamp off in *A*. (*D*) Schematics explaining two different regions regarding dissociation of water clusters. Under light, vapor temperatures drop sharply (Region I) near surface due to dissociation of clusters. A flat region (Region II) exists due to super saturation of water vapor. These features are not seen in thermal evaporation. (*E* and *F*) Transmission spectra above water surface at different heights plotted, for different heights but same sample (*E*), and same height but different samples (*F*). Surface temperature is marked down. In *E*, spectra are shifted for clarify, and all shifts are within 0.5% of transmittance changes. Absolute transmittance data are shown in *F*. For pure water, absorption peak does not change. For pure-PVA and PVA-ppy samples, both blue and red shifts are observed progressively away from the sample surface.

rapidly across the density variation region over a distance of around 3 to 7 Å (40, 41), leading to a large electric field gradient (Fig. 4*A*). Although this field gradient is similar to that in the photoelectric effect (42–44), a significant difference is that the water molecules themselves are neutral. However, water is polar, and the single water dipole moment is around 1.8D (Debye) and increases to ~2.8D in water clusters (35), suggesting an effective charge separation of ~0.5 Å. Such charge separation under the large electric field gradient at the interface leads to a net force on the molecule, i.e., the quadrupole force (39). When the force points outward during the cycle of the time-varying field, the water clusters can be driven off the liquid surface. The difference of the photon energy $\hbar\omega$ to the bonding energy Δ of a water cluster to the surrounding water $\hbar\omega - \Delta$ is converted into the kinetic energy of the molecular cluster (Fig. 4*B*). The bonding energy Δ consists of multiple bonds of the cluster with the surrounding, $\Delta \sim n\Delta_1$, where n is the number of bonds and Δ_1 is the average energy of one bond of the cluster with the surrounding water molecules.

Transport of Molecular Clusters. After a molecular cluster is cleaved off the surface, the clusters will collide with other vapor and air molecules, changing their directions and/or breaking up the molecules in the cluster (Fig. 4*C*) or recondensing onto water or PVA molecules. The molecular-collision breaking-up events are infrequent since the average thermal energy is $k_B T \sim 0.026$ eV at room temperature, while the hydrogen bonds between molecules in the cluster is $E_1 \sim 0.22 - 0.26$eV. The lifetime τ_c for breaking up one molecule is $\exp\left(\frac{E_1}{k_B T}\right) N \sim 10^4 N$ times longer than the regular molecular collision time τ of the order of a nanosecond, where N is the total number of molecules in a cluster. The clusters may change their direction due to momentum exchange with air molecules after each collision. We can estimate the average distance between breaking up one molecule from the cluster as $\Lambda\sqrt{\tau_c/\tau}$, where Λ is the mean free path between collisions, which is ~100 nm for air molecules (45). It means the breaking up events will happen between 10 and 1,000 μm, considering that the molecule clusters have multiple molecules and different initial velocities. Heat is absorbed in this region, leading to a sharp temperature drop close to the sample surface (Region I). After the vapor becomes saturated, the breakup and recondensation of water molecules can simultaneously happen, explaining the flat region we observe in Fig. 3 *A*–*C* (Region II). If the clusters are cleaved deep inside the hydrogel, they can also recondense and release heat (Fig. 4*C*). This process can be called the internal photomolecular effect, which is also responsible for the observed absorption in freeze-thawed samples (Fig. 1*D*). The cluster dissociation in air leads to cooling (Fig. 3*A*), which can be called the external photomolecular effect. For super-thermal

Downloaded from https://www.pnas.org by CAS DALIAN INSTITUTE CHEMICAL PHYSICS on July 29, 2025 from IP address 119.78.131.176.

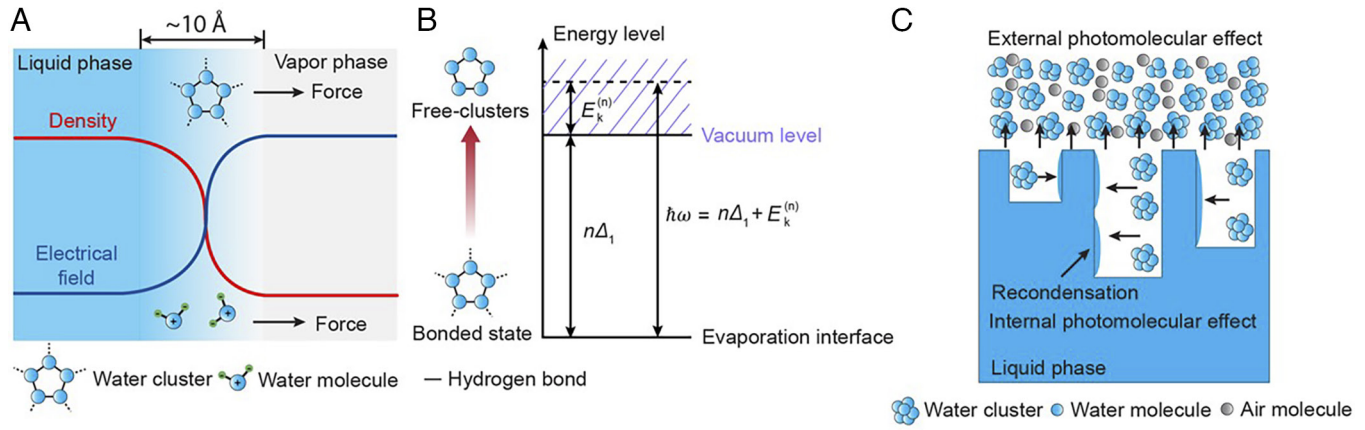

Fig. 4. Conceptual picture of the photomolecular effect. (*A*) Plausible microscopic mechanism for the photomolecular effect at the liquid water–vapor interface. The liquid water–vapor interfacial region is ~10 Å. Over similar distance, the electrical field also changes rapidly, creating a large electrical field gradient, acting on water clusters. The quadrupole potential generates a large force on the cluster and breaks off the cluster during the cycle when the force points to the vapor phase. (*B*) Energy diagram of the photomolecular effect. A photon with an energy ($\hbar\omega$) larger than the bonding energy (Δ_1 is the average bonding energy per bond and *n* the number of bonds) between the water cluster and the remaining water liquids can cleave off the water cluster. Excess energy is converted into the kinetic energy of the clusters. (*C*) Interplay between water clusters and structure. After the cluster leaves the interface, it can recondense inside the hydrogel pores (internal photomolecular effect), generating heat. Water clusters leaving the hydrogel is the external photomolecular effect.

evaporation, one needs to optimize the structures to minimize the internal photomolecular effect.

Conclusions

We hypothesize the existence of the photomolecular effect: Photons cleave off water clusters from the surface region. Experimental evidence supporting this picture include the following: 1) Partially wetted hydrogels become absorbing in the visible spectral range, where the absorption by both the water and the hydrogel materials is negligible. 2) Illumination of hydrogel under solar or visible-spectrum light-emitting-diode leads to evaporation rates exceeding the thermal evaporation limit, even in hydrogels without additional absorbers. 3) The evaporation rates are wavelength dependent, peaking at 520 nm, while the absorptance in the visible spectrum does not show strong wavelength dependence. 4) Temperature of the vapor phase becomes cooler under light illumination and shows saturation behavior. And 5) vapor phase transmission spectra under light show new features and peak shifts. We further suggest that the driving force for the photomolecular effect comes from quadrupole force acting on the polar water molecules connected by hydrogen-bond, which arise due to the rapid change of the electrical field in the direction perpendicular to the interface as mandated by the Maxwell equations. The photomolecular evaporation can be internal and external, although our study emphasizes the external effect, leading to an increased evaporation rate above the thermal evaporation limit.

We want to emphasize that our physical picture is a reasonable hypothesis that can explain the experimental observations, and its correctness awaits further testing by the community. We have yet to understand why the effect happens at 520 nm, where water is almost least absorbing. However, we believe the experimental observations clearly show direct light evaporation processes which explain many past observations of the above thermal limit evaporation under solar radiation. Modeling of such a process has a long way to go, considering the complexity of water itself. Our observations lead us to question whether this effect happens widely in nature, such as in clouds, fogs, ocean and soil surfaces, plant transpiration, and other liquids. Answering these questions calls for collaborations from researchers from different fields.

Materials and Methods

Preparation of Freeze-thawed and Free-dried Pure-PVA samples.
PVA-hydrogel. PVA powder was dissolved in DI water under vigorous stirring with a water bath at 90 °C for 5 h to make a 20 wt% solution. Then, 5 mL PVA solution (20 wt%), 5 mL DI water, and glutaraldehyde (25 wt%) 125 μL were mixed by a vortex mixer for 2 min at room temperature, followed by bubble removal with a centrifuge at 5,000 RPM for 3 min. Next, 1 mL HCl aqueous solution (1.2M) was added, mixing with gentle shaking. The obtained solution was injected into petri dish molds to desired thickness and diameter. The gelation was carried out for 2 h at room temperature. The PVA gel was immersed in DI water for 24 h to obtain pure PVA hydrogel.
Freeze-thaw and freeze-dry. The purified PVA hydrogel was frozen first in a refrigerator at −20 °C for 6 h. The frozen sample is then moved onto a chilled metal block at −40 °C (which leads to an initial cooling rate > 5 K/min) for 2 h. After that, the sample is thawed in the open air. The thawed sample is refrozen on the chilled metal block at −40 °C for 2 h and thawed again in the open air to repeat the freeze–thawing process. To obtain the freeze-thawed sample, the freeze-thawing processes were repeated 1~5 times. The obtained freeze-thawed pure PVA samples (*SI Appendix*, Fig. S1 *A* and *B*) are stored inside a humid glass container for future use. To make freeze-dried PVA samples, the above freeze-thawed samples, after three freeze-thawing cycles, are placed on a chilled metal bulk maintained at −60 °C by liquid nitrogen for 2 h. Next, the samples are freeze-dried at 0 °C and 5.2 mTorr in a home-built freeze-drier for 48 h. The obtained freeze-dried pure PVA samples (*SI Appendix*, Fig. S1 *C* and *D*) are stored inside a sealed dry glass container

Preparation of Freeze-dried PVA Samples with PPy Absorber. To prepare PPy, 0.228g of APS particles was dissolved in 20 mL deionized (DI) water. In addition, 0.69 mL pyrrole was uniformly mixed with 20 mL DI water by a vortex mixer for 5 min. The APS solution and the pyrrole solution were added dropwise to 50 mL 1.2 M HCl aqueous solution stirred with a magnetic stirrer. The polymerization was carried out for 5 min and quenched with DI water. The as-prepared PPy is purified by filtration and washed using DI water three times. The purified PPy was then well dispersed in DI water by sonication to form PPy solution (20 g/L). Next, PVA aqueous solution (20 wt%) 5 mL, glutaraldehyde (25 wt%) 125 μL, and PPy aqueous solution (20 g/L) 5 mL were mixed by sonication for 10 min, followed by removing the bubbles with a centrifuge at 3,000 RPM for 5 min. Next, HCl aqueous solution (1.2M) 1 mL was added, mixing with gentle shaking. The obtained solution was injected into petri dish molds. The gelation was carried out for 2 h at room temperature. The obtained PVA-ppy gel was immersed in DI water for 24 h to clean the gel. The freeze-thaw and freeze-dry processes are the same as pure PVA samples. The obtained freeze-dried PVA-ppy samples are stored inside a sealed dry glass container. *SI Appendix*, Fig. S1 *E* and *F* show photos of the samples.

Preparation of PVA-Carbon Sample. Because the original carbon paper (AvCarb MGL190 obtained from Fuel Cell Earth) is a little hydrophobic and its pore size is too

Downloaded from https://www.pnas.org by CAS DALIAN INSTITUTE CHEMICAL PHYSICS on July 29, 2025 from IP address 119.78.131.176.

large to hold the PVA solution, and its absorptance is relatively low (about 75%), we first treated the carbon paper using a PVA and PPy mixture solution. A 1 ml PVA aqueous solution (20 wt%) was mixed with 2 mL PPy aqueous solution (concentration 20 g/L) by a vortex mixer for 2 min, and the bubbles were removed with a centrifuge at 3,000 RPM for 3 min. The obtained solution was dropwise and uniformly distributed onto the carbon paper (diameter 35 mm, thickness 0.19 mm). The wet carbon is dried in open air inside a fume hood. The physically cross-linked PVA will partially fill the big pores in the carbon paper and binder the PPy particles to improve the paper's absorptance up to 95% (*SI Appendix*, Fig. S9*B*). In the next step, the pure PVA layer is coated onto the above-treated carbon paper. PVA aqueous solution (20 wt%) 5 mL, DI water 5 mL, and glutaraldehyde (25 wt%) 125 μL were mixed with a vortex mixer for 2 min, and bubbles were removed with a centrifuge at 3,000 RPM for 3 min. After the carbon paper surface was dry, HCl aqueous solution (1.2M) 1 mL was added to the prepared PVA solution, mixing with gentle shaking for 5 min. Next, 1 mL of the obtained PVA solution is uniformly coated onto the carbon paper. The polymerization was carried out for 2 h, and the cleaning of the as-prepared PVA-carbon sample was the same as pure PVA samples. The obtained PVA-carbon samples are stored inside a water container before testing. *SI Appendix*, Fig. S1 *G* and *H* show photos of the samples.

Sample Characterization. We used SEM and confocal microscopy (*SI Appendix*, Notes S2 and S3) to investigate the dry and wet freeze-dried hydrogel samples (Fig. 1 *A* and *B* and *SI Appendix*, Fig. S2), respectively. We also used DSC to measure the latent heat of hydrogel (*SI Appendix*, Note S4 and Fig. S3 *A*–*C*). Meanwhile, we used TGA to estimate the decomposition temperatures of the hydrogel samples (*SI Appendix*, Note S5 and Fig. S2*D*). The details of these measurements are available in *SI Appendix*, Notes S4 and S5.

UV-VIS-NIR Absorptance Measurement. We used the Cary 5000 UV-VIS-NIR spectrometer coupled to an integral sphere (Internal DRA 250) to measure the diffuse reflectance R and transmittance T, from which we calculated the absorptance with A = 1-R-T (*SI Appendix*, Note S6). For the reflectance measurement, the sample is placed at the backport of the integral sphere (Fig. 1*C*). For transmittance measurement, the sample is placed at the entrance port of the integral sphere. Each measurement is carried out in the order of transmittance/reflectance/ transmittance, with the third measurement done to make sure that the sample has not changed during the measurements. The reference background spectrum is taken with the backport replaced with a diffuser provided with the integral sphere. The details of all measurement methods are available in *SI Appendix*, Fig. S4 and Note S6, including uncertainty estimations. And the detailed spectra of different samples are available in *SI Appendix*, Fig. S5–S7.

Evaporation Rate Measurement. The samples of the same size as the water container are tightly fixed at the mouth of the water container, where its top surface is at the same height level as the water container. These samples are already immersed in water and fully swollen before they are used for evaporation testing. This arrangement avoids the evaporation from the sidewall of the sample, on the one hand, preventing recondensation on the container wall that could happen when the sample is below the top edge of the water container on the other hand. The details of the setup for the evaporation rate measurement are available in *SI Appendix*, Fig. S8. To minimize heat losses, the sample stages are carefully insulated using PU foam of about 1 cm in thickness. Meanwhile, to avoid the excess light absorption by PU foam, we used aluminum foil to package the PU foam. For LED-driven evaporation, no thermal insulation was used for the sample stage since we found little difference between with and without insulation. To avoid light absorption by the support structure, all the support structure holding the sample stage is made by gluing the glass slides using clear glue (Krazy super glue). Natural evaporation rates are subtracted from the reported final evaporation rate under light. Unlike previous reports (5, 10), none of our samples showed higher evaporation under dark conditions, which we suspect is due to the difference of hydrophilicity of the internal structures as we observed the sample surfaces are always covered with water in dark conditions. The details of all measurement methods are available in *SI Appendix*, Figs. S8 and S10 and Note S7, including uncertainty estimations.

Temperature Measurements. For temperature measurement, we used both a thermocouple and an IR microscope. To use an IR camera to measure the vapor phase temperature distribution, we use a very thin glass slide (0.1 mm in thickness) as a thermal emitter for the IR camera to aim at *SI Appendix*, Fig. S11. Measuring temperature using thermocouples under light needs special attention. To measure the temperature profile in the height direction, it is essential to avoid heat conduction along the length of the thermocouple, which can average out steep temperature variations in the height direction. We used K-type thermocouple (Omega fine wire thermocouple CHAL-0005, 125 μm) shaped into a U-shape (*SI Appendix*, Fig. S12) with a horizontal length of 20 mm to minimize heat conduction loss from the junction along the thermocouple wire, which could also smear out temperature gradient. The details of all measurement methods are available in *SI Appendix*, Note S8, including uncertainty estimations.

Direct Transmission Spectrum of Vapor Phase. We measured the transmission spectrum in the vapor phase at different heights on pure-PVA, PVA-ppy surfaces, and pure water surfaces at different heights when they were subjected to green light (520 nm). The measured spectra are illustrated in *SI Appendix*, Fig. S14 and provided as data files (*SI Appendix*, Tables S4–S7) since the spectra are rich in information and cannot be easily deciphered at this stage. We have explained some main features that clearly show clusters' existence in the main text. The normalization sometimes leads to over 100% due to environmental drift. The details of all measurement methods are available in *SI Appendix*, Note S9, including uncertainty estimations.

Electrical Heating. To demonstrate purely thermal evaporation does not lead to two-stage evaporation, we used electrical heating to raise the hydrogel's temperature (*SI Appendix*, Fig. S10). The main challenges for this approach are 1) the heating should be nearly uniformly distributed while still allowing water to permeate as in solar irradiation, and 2) the heater should be placed as close as possible to surface. We tested different ways to heat the sample electrically and eventually settled on hand-made mesh heaters. The mesh heaters are made from nichrome wires 0.127 mm in diameter, with spacing between wires 0.200 mm. The heaters are embedded into different depths of PVA-ppy hydrogel during the sample preparation. Results from placing the heater at different distance from the surface are also presented. See *SI Appendix*, Fig. S10 and Tables S2 and S3.

Data, Materials, and Software Availability. All study data are included in the article and/or supporting information.

ACKNOWLEDGMENTS. We would like to thank Ms. Hongxia Zeng, who contributed to sample fabrication from 1/2019 to 10/2019, and thank Prof. Guihua Yu and his group members Dr. Fei Zhao, Xingyi Zhou, and Youhong Guo for demonstrating PVA-ppy sample fabrication in 2019. We thank the following people for discussion and help during this work: Dr. Jungwoo Shin (fabricated a homemade freeze-dryer with help of Y.T. and M.A.), Dr. Yoichiro Tsurimaki (trained Y.T. to use the UV-VIS spectrometer), Dr. Yi Huang (helped Y.T. use the UV-VIS spectrometer), Dr. Xiaoyu Chen (did sample surface treatment), Dr. Xin Qian (helped Y.T. make PVA-carbon sample), Qichen Song, Dr. Zhiwei Ding, and Buxuan Li. We would like to thank Professor Evelyn Wang and her group members Lenan Zhang, Geoffrey Vaartstra, Carlos Marin and Chad Wilson for discussion. G.C. also thanks Prof. Z. G. Suo for discussion on hydrogel. All of Y.T.'s work was done at MIT, his first-year post-doc fellowship was supported by Shanghai Jiao Tong University. M.A. was partially supported by a postdoctoral fellowship from Canada's Natural Sciences and Engineering Research Council. G.C. especially thanks MIT for its support.

Author affiliations: [a]Department of Mechanical Engineering, Massachusetts Institute of Technology, Cambridge, MA 02139; and [b]School of Mechanical Engineering, Shanghai Jiao Tong University, Shanghai 200240, China

Author contributions: Y.T. carried out the majority of experiments throughout the whole duration of the project commenced on 1/2019; J.Z. participated in the research from 1/2019-7/2020 via sample fabrication and characterization, including observing the wavelength dependence of LEDs driven PVA-PPy hydrogel evaporation, and measuring the temperature profile in the vapor region, and observing the flat temperature region; S.L. contributed to sample fabrication and characterization throughout whole duration of the work; M.A. contributed to the work through making different samples from PVA starting 04/2020 and contributed to data collection and sample characterization for data reported in the paper; X.Z. supervised the research during GC's absence in 1/2021-6/2021 and thereafter co-supervised the hydrogel evaporation experiments; X.Z. guided the fabrication of all PVA samples, suggested and supervised details of the pure PVA evaporation experiments and the backside optical heating experiments to validate the photon-induced evaporation, and contributed to data interpretation; G.C. initiated and supervised the research except an absence from middle January 2021 to the end of June 2021; G.C. organized sample fabrication effort and suggested early experiments on wavelength and intensity dependence, electrical heating, IR image in vapor phase and thermocouple mapping to validate the concept of photon-induced evaporation and led data interpretation, and supervised details of the experiments; In July 2021, G.C. conceived the theoretical picture of photomolecular effect, suggested experiments (hydrogel absorptance and vapor spectra) to validate the photomolecular concept and led data interpretation, and supervised details of the experiments; G.C. led the writing of the manuscript, working closely with Y.T.; and all team members contributed to manuscripts via discussion, figure making, and proofreading.

Downloaded from https://www.pnas.org by CAS DALIAN INSTITUTE CHEMICAL PHYSICS on July 29, 2025 from IP address 119.78.131.176.

1. H. Ghasemi *et al.*, Solar steam generation by heat localization. *Nat. Commun.* **5**, 1–7 (2014).
2. Z. Wang *et al.*, Bio-inspired evaporation through plasmonic film of nanoparticles at the air–water interface. *Small* **10**, 3234–3239 (2014).
3. P. Tao *et al.*, Solar-driven interfacial evaporation. *Nat. Energy* **3**, 1031–1041 (2018).
4. L. Zhou *et al.*, 3D self-assembly of aluminium nanoparticles for plasmon-enhanced solar desalination. *Nat. Photonics* **10**, 393–398 (2016).
5. F. Zhao *et al.*, Highly efficient solar vapour generation via hierarchically nanostructured gels. *Nat. Nanotechnol.* **13**, 489–495 (2018).
6. G. M. Hale, M. R. Querry, Optical constants of water in the 200-nm to 200-μm wavelength region. *Appl. Optics* **12**, 555–563 (1973).
7. T. A. Cooper *et al.*, Contactless steam generation and superheating under one sun illumination. *Nat. Commun.* **9**, 1–10 (2018).
8. T. P. Otanicar, P. E. Phelan, R. S. Prasher, G. Rosengarten, R. A. Taylor, Nanofluid-based direct absorption solar collector. *J. Renew. Sustain. Energy* **2**, 033102 (2010).
9. O. Neumann *et al.*, Solar vapor generation enabled by nanoparticles. *ACS Nano* **7**, 42–49 (2012).
10. F. Zhao, Y. Guo, X. Zhou, W. Shi, G. Yu, Materials for solar-powered water evaporation. *Nat. Rev. Materials* **5**, 388–401 (2020).
11. X. Mu *et al.*, Energy matching for boosting water evaporation in direct solar steam generation. *Solar RRL* **4**, 2000341 (2020).
12. X. Zhou, F. Zhao, Y. Guo, Y. Zhang, G. Yu, A hydrogel-based antifouling solar evaporator for highly efficient water desalination. *Energy Environ. Sci.* **11**, 1985–1992 (2018).
13. Y. Bian *et al.*, Carbonized bamboos as excellent 3D solar vapor-generation devices. *Adv. Mater. Technol.* **4**, 1800593 (2019).
14. H. Wang, R. Zhang, D. Yuan, S. Xu, L. Wang, Gas foaming guided fabrication of 3D porous plasmonic nanoplatform with broadband absorption, tunable shape, excellent stability, and high photothermal efficiency for solar water purification. *Adv. Funct. Mater.* **30**, 2003995 (2020).
15. Y. Guo *et al.*, Tailoring surface wetting states for ultrafast solar-driven water evaporation. *Energy Environ. Sci.* **13**, 2087–2095 (2020).
16. T. Gao, X. Wu, Y. Wang, G. Owens, H. Xu, A hollow and compressible 3D photothermal evaporator for highly efficient solar steam generation without energy loss. *Solar RRL* **5**, 2100053 (2021).
17. Y. Shi *et al.*, Plasmonic silver nanoparticles embedded in flexible three-dimensional carbonized melamine foam with enhanced solar-driven water evaporation. *Desalination* **507**, 115038 (2021).
18. X. Zhang, Y. Peng, L. Shi, R. Ran, Highly efficient solar evaporator based on a hydrophobic association hydrogel. *ACS Sustain. Chem. Eng.* **8**, 18114–18125 (2020).
19. Z. Dong, C. Zhang, H. Peng, J. Gong, Q. Zhao, Modular design of solar-thermal nanofluidics for advanced desalination membranes. *J. Mater. Chem. A* **8**, 24493–24500 (2020).
20. J. Li *et al.*, Over 10 kg m^{-2} h^{-1} evaporation rate enabled by a 3D interconnected porous carbon foam. *Joule* **4**, 928–937 (2020).
21. Y. Tian *et al.*, Carbonized cattle manure-based photothermal evaporator with hierarchically bimodal pores for solar desalination in high-salinity brines. *Desalination* **520**, 115345 (2021).
22. H. Hertz, On an effect of ultraviolet light upon the electric discharge. *Ann. Physik* **31**, 983 (1887).
23. A. Einstein, On a heuristic point of view concerning the production and transformation of light. *Ann. Phys.* **17**, 132–148 (1905).
24. M. S. Jhon, J. D. Andrade, Water and hydrogels. *J. Biomed. Mater. Res.* **7**, 509–522 (1973).
25. T. Ikeda-Fukazawa *et al.*, Effects of crosslinker density on the polymer network structure in poly-N, N-dimethylacrylamide hydrogels. *J. Polymer Sci. B Polymer Phys.* **51**, 1017–1027 (2013).
26. G. Chen, Thermodynamics of hydrogels for applications in atmospheric water harvesting, evaporation, and desalination. *Phys. Chem. Chem. Phys.* **24**, 12329–12345 (2022).
27. E. Yablonovitch, Statistical ray optics. *JOSA* **72**, 899–907 (1982).
28. F. H. Stillinger, Water revisited. *Science* **209**, 451–457 (1980).
29. R. Ludwig, Water: From clusters to the bulk. *Angew. Chem. Int. Ed.* **40**, 1808–1827 (2001).
30. S. W. Benson, E. D. Siebert, A simple two-structure model for liquid water. *J. Am. Chem. Soc.* **114**, 4269–4276 (2002).
31. M. F. Chaplin, A proposal for the structuring of water. *Biophys. Chem.* **83**, 211–221 (2000).
32. F. Weinhold, Quantum cluster equilibrium theory of liquids: General theory and computer implementation. *J. Chem. Phys.* **109**, 367 (1998).
33. Y. R. Shen, V. Ostroverkhov, Sum-frequency vibrational spectroscopy on water interfaces: Polar orientation of water molecules at interfaces. *Chem. Rev.* **106**, 1140–1154 (2006).
34. L. G. M. Pettersson, R. H. Henchman, A. Nilsson, Water–The most anomalous liquid. *Chem. Rev.* **116**, 7459–7462 (2016).
35. J. K. Gregory, D. C. Clary, K. Liu, M. G. Brown, R. J. Saykally, The water dipole moment in water clusters. *Science* **275**, 814–817 (1997).
36. F. Huisken, M. Kaloudis, A. Kulcke, Infrared spectroscopy of small size-selected water clusters. *J. Chem. Phys.* **104**, 17 (1998).
37. B. Zhang *et al.*, Infrared spectroscopy of neutral water clusters at finite temperature: Evidence for a noncyclic pentamer. *Proc. Natl. Acad. Sci. U.S.A.* **117**, 15423–15428 (2020).
38. C. C. Pradzynski, R. M. Forck, T. Zeuch, P. Slavíček, U. Buck, A fully size-resolved perspective on the crystallization of water clusters. *Science* **337**, 1529–1532 (2012).
39. J. D. Jackson, *Classical Electrodynamics* (Wiley, ed. 3, 1998).
40. L. X. Dang, T.-M. Chang, Molecular dynamics study of water clusters, liquid, and liquid–vapor interface of water with many-body potentials. *J. Chem. Phys.* **106**, 8149 (1998).
41. J. Alejandre, D. J. Tildesley, G. A. Chapela, Molecular dynamics simulation of the orthobaric densities and surface tension of water. *J. Chem. Phys.* **102**, 4574 (1998).
42. S. Hüfner, *Photoelectron Spectroscopy: Principles and Applications* (Springer Berlin Heidelberg, 2003).
43. P. J. Feibelman, Surface electromagnetic fields. *Prog. Surf. Sci.* **12**, 287–407 (1982).
44. A. Liebsch, *Electronic Excitations at Metal Surfaces* (Springer US, 1997).
45. G. Chen, *Nanoscale Energy Transport and Conversion: A Parallel Treatment on Electrons, Molecules, Phonons, and Photons* (Oxford University Press, 2005).

Downloaded from https://www.pnas.org by CAS DALIAN INSTITUTE CHEMICAL PHYSICS on July 29, 2025 from IP address 119.78.131.176.